

Article

Influence of the Fin Shape on Heat Transport in Phase Change Material Heat Sink with Constant Heat Loads

Nadezhda S. Bondareva ¹, Mohammad Ghalambaz ^{2,3} and Mikhail A. Sheremet ^{1,*}

¹ Laboratory on Convective Heat and Mass Transfer, Tomsk State University, 634050 Tomsk, Russia; bondarevans@mail.tsu.ru

² Metamaterials for Mechanical, Biomechanical and Multiphysical Applications Research Group, Ton Duc Thang University, Ho Chi Minh City 758307, Vietnam; mohammad.ghalambaz@tdtu.edu.vn

³ Faculty of Applied Sciences, Ton Duc Thang University, Ho Chi Minh City 758307, Vietnam

* Correspondence: sheremet@math.tsu.ru

Abstract: Nowadays, the heat transfer enhancement in electronic cabinets with heat-generating elements can be achieved using the phase change materials and finned heat sink. The latter allows to improve the energy transference surface and to augment the cooling effects for the heat sources. The present research deals with numerical analysis of phase change material behavior in an electronic cabinet with an energy-generating element. For an intensification of heat removal, the complex finned heat sink with overall width of 10 cm was introduced, having the complicated shape of the fins with width of 0.33 cm and height $H = 5$ cm. The fatty acid with melting temperature of $46\text{ }^{\circ}\text{C}$ was considered as a phase change material. The considered two-dimensional challenge was formulated employing the non-primitive variables and solved using the finite difference method. Impacts of the volumetric heat flux of heat-generating element and sizes of the fins on phase change material circulation and energy transference within the chamber were studied. It was shown that the presence of transverse ribs makes it possible to accelerate the melting process and reduce the source temperature by more than $12\text{ }^{\circ}\text{C}$ at a heat load of 1600 W/m . It should also be noted that the nature of melting depends on the hydrodynamics of the melt, so the horizontal partitions reduce the intensity of convective heat transfer between the upper part of the region and the lower part.

Keywords: electronics cooling; phase change material; complicated finned heat sink; natural convection; heat-generating element; numerical results



Citation: Bondareva, N.S.; Ghalambaz, M.; Sheremet, M.A. Influence of the Fin Shape on Heat Transport in Phase Change Material Heat Sink with Constant Heat Loads. *Energies* **2021**, *14*, 1389. <https://doi.org/10.3390/en14051389>

Academic Editors: Yulong Ding and Adrián Mota Babiloni

Received: 17 December 2020

Accepted: 24 February 2021

Published: 3 March 2021

Publisher's Note: MDPI stays neutral with regard to jurisdictional claims in published maps and institutional affiliations.



Copyright: © 2021 by the authors. Licensee MDPI, Basel, Switzerland. This article is an open access article distributed under the terms and conditions of the Creative Commons Attribution (CC BY) license (<https://creativecommons.org/licenses/by/4.0/>).

1. Introduction

In recent decades, the production of mobile devices and electronic gadgets has been actively developing. At the same time, high-tech solutions for cooling systems are required. Heat sinks with a simple design made of highly heat-conducting materials heat up quickly enough and require long-term cooling. To enhance the process of heat dissipation, active systems are used, such as liquid cooling systems, fans, systems based on phase transitions involving the evaporative or solid-liquid phase changes.

In traditional air cooling systems, the ratio of volume to surface area and the aerodynamic characteristics of the profile are important factors for performance [1–3]. A growth of mass per volume unit results in a rise of the effective heat capacity, while an increase in the surface by creating a profile of a more complex shape leads to an intensification of heat exchange with the environment. Such heat sinks are usually used with active systems, for instance, fans, liquid pumps, and others. Therefore, the effect of geometry changing on the heat dissipation efficiency must be studied, taking into account the intensity of the forced convection. Comparison of active cooling systems based on a pin-fin cooler and plate-fin heat sink were carried out in [4]. It was shown that at a constant pumping power, the pin-fin heat sinks have a higher heat dissipation capacity than plate-fin heat sinks.

Another effective way to increase the surface area of a structure is to use the metal foam heat sinks [5–8].

Radiator systems with phase change materials (PCM) allow converting a large volume of sensible heat into latent energy at fixed temperatures. In this regard, much attention has recently been paid to research devoted to the melting materials behavior under the heaters influence in enclosures. The shape of the heat-dissipating profile allows not only to increase the area of contact with the material for its greatest melting but also to promote the development of circulation of the melt to enhance heat transfer at the phase transition boundary. Therefore, when working out the melting challenges, it is necessary to analyze an impact of the surface profiles shape on the hydrodynamics [9–12]. Natural convection is responsible for the circulation of the melt in the case of passive cooling systems; therefore, it is significant to assess the influence of the heat flux and the size of the region.

Coolers based on PCMs have higher effective heat capacity, do not take up much volume, and do not require an additional power supply. Phase change materials can be considered as some groups of organic compounds: fatty acids and eutectics with the melting points in the range 30–68 °C and latent heat in the range from 150.6 to 211.6 kJ/kg; n-alkanes the melting temperature from –9.6 °C and L_m to 252 kJ/kg; paraffin with melting temperatures up to 108 °C; as well as some inorganic compounds [13,14]. The convenience and practicality of using PCM have found wide application in different industries including electronics, aerospace engineering, solar energy, construction, etc. [15–17].

A large number of numerical and experimental research studies are devoted to this topic; however, a large number of factors affecting a complex thermohydrodynamic process give rise to a wide variety of energy transport problems under conditions of phase transformations [18–24]. In [9], finned heat sink filled with n-eicosane was experimentally examined at different heating modes. It has been shown that at constant heat loads of 5 W, the addition of PCM reduces the heat sink temperature by more than 5°. Moreover, the addition of metal fins in the profile also contributes to a decrease in temperature by several degrees. Pin-finned configuration of the heat sink was considered as a passive cooling system in [25]. Paraffin RT-44 was used as phase change material. The geometry of the heat sink plays an important role in performance, namely, an increase in the fin height leads to an increase in the critical time for various critical temperatures (at $T_{cr} = 60$ °C, $T_{cr} = 70$ °C and $T_{cr} = 80$ °C). It has been shown that, in some cases, T_{cr} increases by more than 20 times in comparison with the case of a cooler without fins, which is achieved by an increase in the fins number and its elongation. In [10], the influence of the number of horizontal ribs and their length were analyzed numerically. New correlations were obtained for the liquid fraction in the region with horizontal edges depending on the Stefan, Rayleigh, and Fourier numbers, as well as the geometric parameters of the heat sink. It has been shown that the elongation of the ribs significantly accelerates the melting process. Heat transfer between PCM and the metal profile depends significantly on the ratio of the PCM volume to the profile volume, as well as the geometric parameters of the solid phase, such as thickness, shape, and number of fins [26–31]. An increase in the number of fins accelerates the melting process, while a decrease in fins thickness increases the source temperature [27]. In the study [26], the PCM-based heat sinks with different shapes of the pin fins were examined. Tall fins with rectangular, circular, and triangular sections were considered. The triangular-shape pin fins allow reducing the element temperature compared to other analyzed shapes. Two models of passive cooling were considered in [11]; namely, a cooler with vertical plate fins and a tree shape cooler made of aluminum. It was demonstrated that thermal convection significantly enhances the energy transfer. The use of a branched profile design leads to the formation of many vortex cells with an intensification of heat transfer.

Another way to augment the energy transport and to speed up the melting or solidification process is the use of metal foams [32–36]. The significant attenuation of natural convection is neutralized by the high heat conductivity of the foam. Shell and tube latent heat thermal storage device in two-dimensional approximation was considered numerically

in [37]. The outer tube was filled with the metal foam with rubitherm 58 (RT-58). Here, the metal foam allows strengthening the phase change processes of the material significantly. In [38], the copper profile with outer fins for a rectangular chamber was examined. The domain was considered for three different configurations, including a rectangular copper basement, a cavity filled with pure PCM, and a cavity filled with paraffin and metal foam. Comparison of the temperature at the heating surface has shown that the surface temperature is 14 degrees lower when using a PCM-based cooler in comparison with a copper basement cooler. The use of metal foam also reduces the maximum surface temperature by more than 4 degrees by raising the heat conductivity in the paraffin. The effect of the pore-scale on heat storage characteristics was assessed in [8]. Reducing porosity increases the heat transfer in the wax. Special effect can also be achieved by using the metal foam with graded porosity or finned-metal foam heat sinks [5,39,40], by increasing the porosity towards the source, the performance of the heat sink can be increased [5].

The effect of convective energy transport in porous media is determined by the porosity of the foam. In [41], the authors considered PCM with metal foam in an aluminum casing with different casing orientations. It was shown that before the beginning of melting, the surface temperature does not depend on the orientation. With a growth in the melting region, the minimum temperature is observed at a zero inclination angle when the heated is located below. Thus, with the melting of PCM, thermal convection in the melt develops. However, an appearance of metal foam contributes to an increase in thermal conductivity and, at the same time, a decrease in the strength of convective energy transport.

Despite the large number of numerical works devoted to this issue, the main difficulty lies in the construction of an effective numerical model describing the complex thermal processes. The presence of a movable boundary significantly complicates the modeling process, and most of the numerical studies present the heat transfer in regions with simple geometry, do not take into account the volumetric heat generation. As a rule, the technique with conditions of constant temperature or constant heat flux at the boundaries illustrates the thermal boundary conditions, that does not always coincide with real physical conditions and has the limited application.

This study is devoted to the effect of the intensity of convective energy transference on the melting processes of lauric acid inside a copper heat sink, depending on its geometry. An element with constant volumetric energy production was used as a heater. The radiator has vertical plate fins with additional transverse fins, the length of which was varied. The significance and novelty of this investigation consist in a consideration of a system with complex geometry using a source of volumetric heat generation and external Newtonian cooling, as well as an assessment of the influence of hydrodynamics on the melting process.

2. Basic Equations

The rectangular system presented in Figure 1, in the form of a metal profile with internal plate fins of finite thickness in the presence of additional transverse fins that affect heat dissipation and hydrodynamic phenomenon in the melt, is considered. The compartments between the fins are filled with phase change material. A rectangular element of volumetric energy production is in contact with the lower wall of the heat sink. The system is cooled through air convection on the top and side walls of the chamber; the bottom wall is considered to be thermally insulated. The heat source is thermally insulated from all sides, except for the top wall where the heater is in contact with the metal substrate. At the initial time moment, the entire system is cooled to ambient temperature, and the source begins to heat up, releasing an equal amount of energy at each moment of time. It is assumed that the change in the PCM volume during the phase transition is negligible.

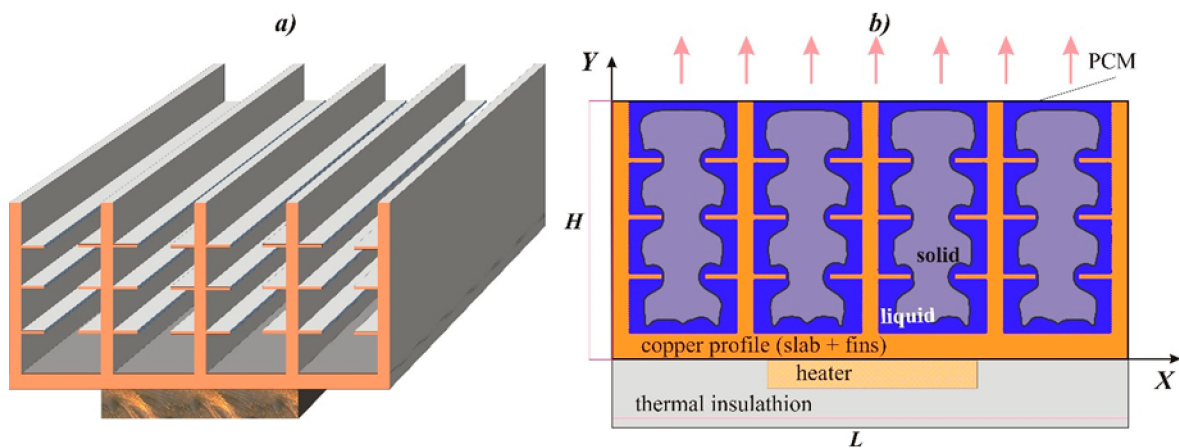


Figure 1. Metal heat sink saturated with PCM (phase change material) and heated from the source. (a) 3D shape of the heat sink with the source of volumetric heat generation, (b) considered 2D model with PCM.

The height of the cooler, including the substrate and the fins, is H , the width is $L = 2 \times H$, vertical fins are extended along with the entire height, horizontal equidistant fins of length l are placed on the vertical plates. The profiles with small horizontal fins of different lengths, including $l = H/24$, $l = H/12$, and $l = H/8$, are considered. The source dimensions relative to the heat sink are $4L/3 \times 0.2L$.

The problem of conjugate natural convection in the closed region was solved under an influence of a local heater of constant volumetric energy production, taking into account the phase transitions. The mathematical statement was formulated through the system of Navier–Stokes equations for a viscous incompressible fluid. The buoyancy force was described using the Boussinesq approximation.

Hydrodynamic equations taking into account the thermogravitational convection are [42,43]:

$$\frac{\partial u}{\partial x} + \frac{\partial v}{\partial y} = 0, \quad (1)$$

$$\rho \left(\frac{\partial u}{\partial t} + u \frac{\partial u}{\partial x} + v \frac{\partial u}{\partial y} \right) = - \frac{\partial p}{\partial x} + \mu \left(\frac{\partial^2 u}{\partial x^2} + \frac{\partial^2 u}{\partial y^2} \right), \quad (2)$$

$$\rho \left(\frac{\partial v}{\partial t} + u \frac{\partial v}{\partial x} + v \frac{\partial v}{\partial y} \right) = - \frac{\partial p}{\partial y} + \mu \left(\frac{\partial^2 v}{\partial x^2} + \frac{\partial^2 v}{\partial y^2} \right) + \rho g \beta (T - T_m). \quad (3)$$

Taking into account the presence of a moving boundary between the solid region and the liquid region for the PCM, the equation of heat conduction for the solid material, and the energy equation for the melt, taking into account the convective terms in the liquid, define the heat dissipation. The energy equations for the PCM (4) and (5), as well as for the profile (6) and the heater (7), have the form:

$$\frac{\partial h}{\partial t} = k_s \left(\frac{\partial^2 T}{\partial x^2} + \frac{\partial^2 T}{\partial y^2} \right), \quad (4)$$

$$\frac{\partial h}{\partial t} + u \frac{\partial h}{\partial x} + v \frac{\partial h}{\partial y} = k_l \left(\frac{\partial^2 T}{\partial x^2} + \frac{\partial^2 T}{\partial y^2} \right), \quad (5)$$

$$\frac{\partial T}{\partial t} = \alpha_1 \left(\frac{\partial^2 T}{\partial x^2} + \frac{\partial^2 T}{\partial y^2} \right), \quad (6)$$

$$\frac{\partial T}{\partial t} = \alpha_2 \left(\frac{\partial^2 T}{\partial x^2} + \frac{\partial^2 T}{\partial y^2} \right) + \frac{Q}{\rho_2 c_2}. \quad (7)$$

To take into account the processes of phase transitions (melting/crystallization), Equations (4) and (5) at the interface are closed by the following conditions: the tem-

perature is equal to the melting temperature $T = T_m$, and the enthalpy has a discontinuity in the transition from one phase to another phase using the following relation:

$$h = \begin{cases} \rho_s c_s T, & T < T_m \\ \rho_s c_s T_m + \rho_l L_f + \rho_l c_l (T - T_m), & T \geq T_m \end{cases} .$$

The energy equations for the material in the enthalpy formulation (4) and (5) were reduced to a unified energy equation using temperature T as a dependent function. To describe the heat transfer from sensible heat to latent heat on the phase transformation line, a smoothing function φ was employed, which characterizes the volume fraction of the melt.

To formulate Equations (1)–(7) in dimensionless form, the following scales were employed. Here, ΔT is set at 60° , and the following ratios are $V_0 = \sqrt{g\beta\Delta TH}$, $X = x/H$, $Y = y/H$, $\Theta = (T - T_m)/\Delta T$, $\tau = tV_0/H$, $\Psi = \psi/HV_0$, $\Omega = \omega H/V_0$.

Dimensionless complexes characterizing the properties of the material, the strength of convective energy transference, the latent heat, and the power of heat generation in the source are as follows: $Ra = g\beta\Delta TH^3/(\nu\alpha)$ is the Rayleigh number, $Pr = \nu/\alpha$ is the Prandtl number, $Ste = L_f/(c_l\Delta T)$ is the Stefan number, $Os = QH^2/(k_2\Delta T)$ is the Ostrogradsky number, to describe the intensity of energy transference with the environment on the upper and side walls of the enclosure, the Biot number was used $Bi = \gamma H/k$.

The following non-dimensional equations were obtained:

$$\frac{\partial^2 \Psi}{\partial X^2} + \frac{\partial^2 \Psi}{\partial Y^2} = -\Omega, \quad (8)$$

$$\frac{\partial \Omega}{\partial \tau} + U \frac{\partial \Omega}{\partial X} + V \frac{\partial \Omega}{\partial Y} = \sqrt{\frac{Pr}{Ra}} \left(\frac{\partial^2 \Omega}{\partial X^2} + \frac{\partial^2 \Omega}{\partial Y^2} \right) + \frac{\partial \Theta}{\partial X}, \quad (9)$$

$$\zeta(\varphi) \left[\frac{\partial \Theta}{\partial \tau} + U + V \frac{\partial \Theta}{\partial Y} \right] + Ste \cdot \left[\frac{\partial \varphi}{\partial \tau} + U \frac{\partial \varphi}{\partial X} + V \frac{\partial \varphi}{\partial Y} \right] = \frac{\xi(\varphi)}{\sqrt{Ra \cdot Pr}} \left(\frac{\partial^2 \Theta}{\partial X^2} + \frac{\partial^2 \Theta}{\partial Y^2} \right), \quad (10)$$

$$\frac{\partial \Theta}{\partial \tau} = \frac{\alpha_1/\alpha_0}{\sqrt{Ra \cdot Pr}} \left(\frac{\partial^2 \Theta}{\partial X^2} + \frac{\partial^2 \Theta}{\partial Y^2} \right), \quad (11)$$

$$\frac{\partial \Theta}{\partial \tau} = \frac{\alpha_2/\alpha_0}{\sqrt{Ra \cdot Pr}} \left(\frac{\partial^2 \Theta}{\partial X^2} + \frac{\partial^2 \Theta}{\partial Y^2} + Os \right). \quad (12)$$

Here, the function φ takes a value from 0 to 1 depending on the temperature:

$$\varphi = \begin{cases} 0, & T < T_m - \eta \\ \frac{T - (T_m - \eta)}{2\eta}, & T_m - \eta \leq T \leq T_m + \eta \\ 1, & T > T_m + \eta \end{cases} .$$

A smoother transition from one phase to another phase is ensured by replacing the melting point $\Theta = 0$ with a temperature range $-\eta \leq \Theta \leq \eta$ in which a smooth change in thermophysical parameters occurs, which leads to a smooth transition of the values of thermal conductivity $\zeta(\varphi) = k_{s,l} + \varphi(1 - k_{s,l})$ and volumetric heat capacity $\xi(\varphi) = \rho_{s,l}c_{s,l} + \varphi(1 - \rho_{s,l}c_{s,l})$, as well as smooth changes of the material enthalpy at the interface. The value of η was chosen 0.005 and was determined by the size of the mesh used.

In the foregoing physical statement, the system under consideration is located in an environment of constant temperature $\Theta = \Theta_{out}$, while the outer borders $Y = 1$, $X = 0$, and $X = 2$ are cooled by air convection, other boundaries, including the source, are considered to be thermally insulated from the environment. At the initial time, the material has a solid-state ($\Psi = 0$, $\Omega = 0$), and the entire system has the initial temperature that is equal to the ambient temperature Θ_{out} .

For the boundaries of the system under consideration, we have on the upper and side walls of the cooler, the condition of Newtonian cooling with a small heat transfer coefficient is set:

$$0 \leq X \leq 2, Y = 1: \left. \frac{\partial \Theta}{\partial Y} \right|_{Y=1} = -Bi(\Theta_{Y=1} - \Theta_{out});$$

$$X = 0 \text{ and } X = 2, 0 \leq Y \leq 1: \left. \frac{\partial \Theta}{\partial Y} \right|_{X=0} = -Bi(\Theta_{X=0} - \Theta_{out}) \text{ and } \left. \frac{\partial \Theta}{\partial Y} \right|_{X=2} = -Bi(\Theta_{X=2} - \Theta_{out});$$

at the lower boundary of the cooler and the external boundaries of the heater, the thermal insulation condition is used, namely, for $X = 0.6$ and $X = 1.4$, $-0.2 \leq Y \leq 0$, and $0.6 \leq X \leq 1.4$, $Y = -0.2$ one can find $\partial \Theta / \partial \bar{n} = 0$; for PCM boundaries: at the copper radiator surface we have: $\Theta_0 = \Theta_1$, $k_0 \frac{\partial \Theta_0}{\partial Y} = k_1 \frac{\partial \Theta_1}{\partial Y}$; at all boundaries of the molten region, the no-slip condition is used, namely, $\Psi = 0$, and Poisson equation for the stream function is used to define the vorticity value as follows: $\Omega = -\left(\frac{\partial^2 \Psi}{\partial X^2} + \frac{\partial^2 \Psi}{\partial Y^2}\right)$; for the heat source boundaries: the condition of equality of heat fluxes and temperatures at the interface between the source and slab is used: $\begin{cases} \Theta_1 = \Theta_2 \\ k_1 \frac{\partial \Theta_1}{\partial Y} = k_2 \frac{\partial \Theta_2}{\partial Y} \end{cases}$.

3. Numerical Technique

The finite difference technique was employed to work out the resulting set of equations with the above additional conditions [42,43]. The energy conduction equations in the copper cooler, in the source, and the energy equation in the PCM were worked out using the Samarskii locally one-dimensional scheme. The solution of the hydrodynamics equations was carried out in a region bounded by solid surfaces and an isolines of $\Theta = 0$. The latter illustrates the position of the phase change interface. The elliptic equation for the stream function was approximated using the central differences. The obtained system of equations was worked out using the successive over-relaxation algorithm. The vorticity equation and the energy equation were worked out employing the locally one-dimensional Samarskii scheme that allows reducing the two-dimensional problem to the set of one-dimensional problems. To solve the system of discretized equations, the developed in-house computational code written employing C++ programming language was used. High accuracy of the solution was achieved by approximating the terms of the Equations (8)–(12) by difference schemes of the second-order of accuracy and using the detailed fixed grid of 480×200 elements. The dimension of the grid was chosen taking into account the performed mesh sensitivity analysis (see Figure 2) with meshes of 240×100 elements, 480×200 elements, and 720×300 elements. Large differences in the results are observed for the mesh of 240×100 elements, that can be explained by the small thickness of the transverse fins. The results obtained for grids of 480×200 elements and 720×300 elements are practically identical, namely, the difference in the volume of the melt at $t = 35$ min is 0.2%.

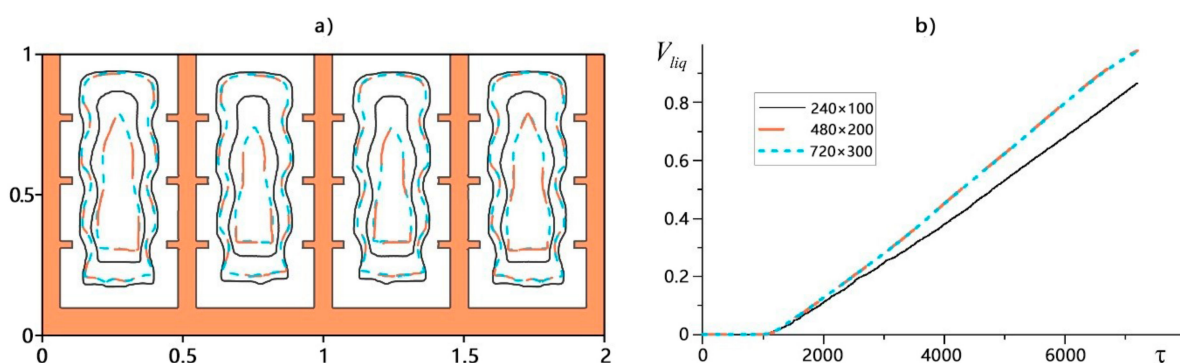


Figure 2. The grid independence test: the phase front location at $t = 25$ and $t = 35$ min (a), as well as a graph of the dependence of the volume fraction of the melt on the dimensionless time (b).

The numerical algorithm was applied to a number of test problems [44–46]. To compare the model results, the experimental problem of melting lauric acid inside a closed system containing an aluminum profile with the finned plate was chosen. The system is heated by water as a heat transfer fluid that circulates in the tubes inside the profile substrate. Figure 3a shows a comparison of the experimental data [44] and the obtained numerical results. In this Figure 3a the black color illustrates the melt, while the white color illustrates the unmelted material shown in the photograph of the region from the side wall of low thermal conductivity; isotherms, obtained numerically, are superimposed on it. Here, the pink isoline is the melting front for $T = T_m$. The problem of melting gallium inside a parallelepiped with two isothermal walls [46] was also considered as a benchmark problem. Figure 3b shows a comparison of the phase change interface location at different times.

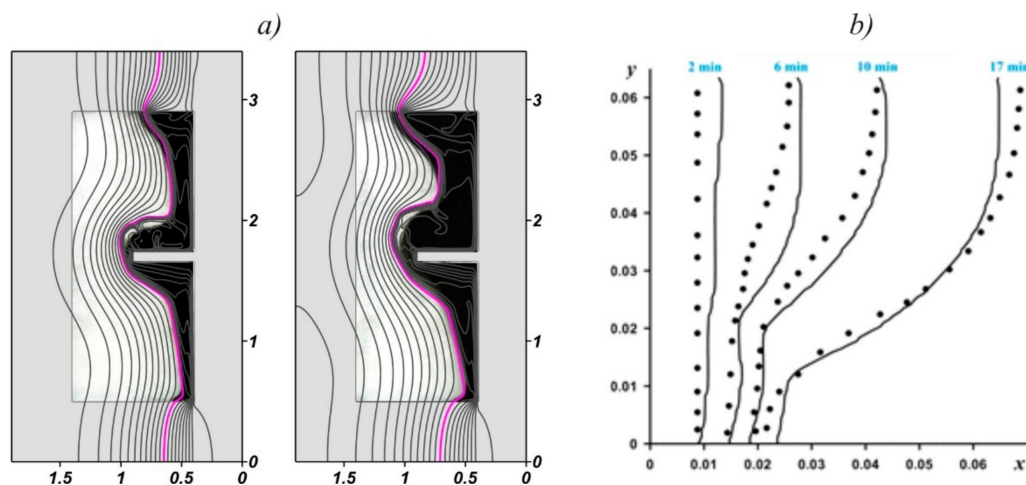


Figure 3. Validation of the developed mathematical model and numerical technique: comparison of calculated outcomes (solid lines) and experimental results (black and white photography) [44] (a); comparison of obtained numerical data (solid line) and experimental data (dots) [46] (b).

4. Results

The performance of such a system depends greatly on the materials chosen. The total effective heat capacity is determined by the density and heat capacity of the materials used and the latent heat of the PCM. Wherein, for the fastest thermal dissipation, the fins of a cooler and the substrate must have a high thermal conductivity. For effective passive cooling, lauric acid [44,45] with a melting temperature of 46 °C, which, in addition to high latent heat, also has a high heat capacity, was chosen as PCM. The melting range in the considered setting using the smoothing function φ is 45.7–46.3 °C. For the profile, a material with high thermal conductivity, copper, was selected, and a silicon element was chosen for the heater. All thermophysical attributes of the system elements are presented in Table 1.

Table 1. Properties of materials.

| Phase Change Material | Lauric Acid [44] | Copper (Radiator) | Silicon (Heat Source) |
|-------------------------------------|--------------------|-------------------|-----------------------|
| T_m , °C | 46 | – | – |
| L_f , kJ/Kg | 187.2 | – | – |
| k_s/k_l , W/(m·K) | 0.16/0.14 | 401 | 148 |
| ρ_s/ρ_l , kg/m ³ | 940/885 | 8900 | 2330 |
| c_s/c_l , J/(kg·K) | 2180/2390 | 385 | 714 |
| μ , Pa·s | 8×10^{-3} | – | – |
| β , 1/K | 8×10^{-4} | – | – |

In this numerical research, the cooler with a cross-section having a height of $H = 5$ cm and a width of $L = 10$ cm is considered. The intensity of source heat generation is varied in the range between 400 and 1600 W/m, which corresponds to the Ostrogradsky number ranged between $Os = 0.169$ and $Os = 0.676$. The Prandtl number for lauric acid is $Pr = 136.6$, and for the selected temperature scale and characteristic scale, the Rayleigh number is $Ra = 9.83 \cdot 10^7$, and the Stefan number is $Ste = 1.3$.

In this formulation, the high Rayleigh number indicates that natural convection of high intensity can be developed in the melt. Therefore, the shape of the finned surface of the profile will significantly affect the thermophysical processes inside the system. The interaction of laminar flows with thermal conductivity in the branches of the profile can lead to both an increase in heat transfer and a decrease in it.

Figure 4 shows the temperature patterns and streamlines for $Os = 0.169$.

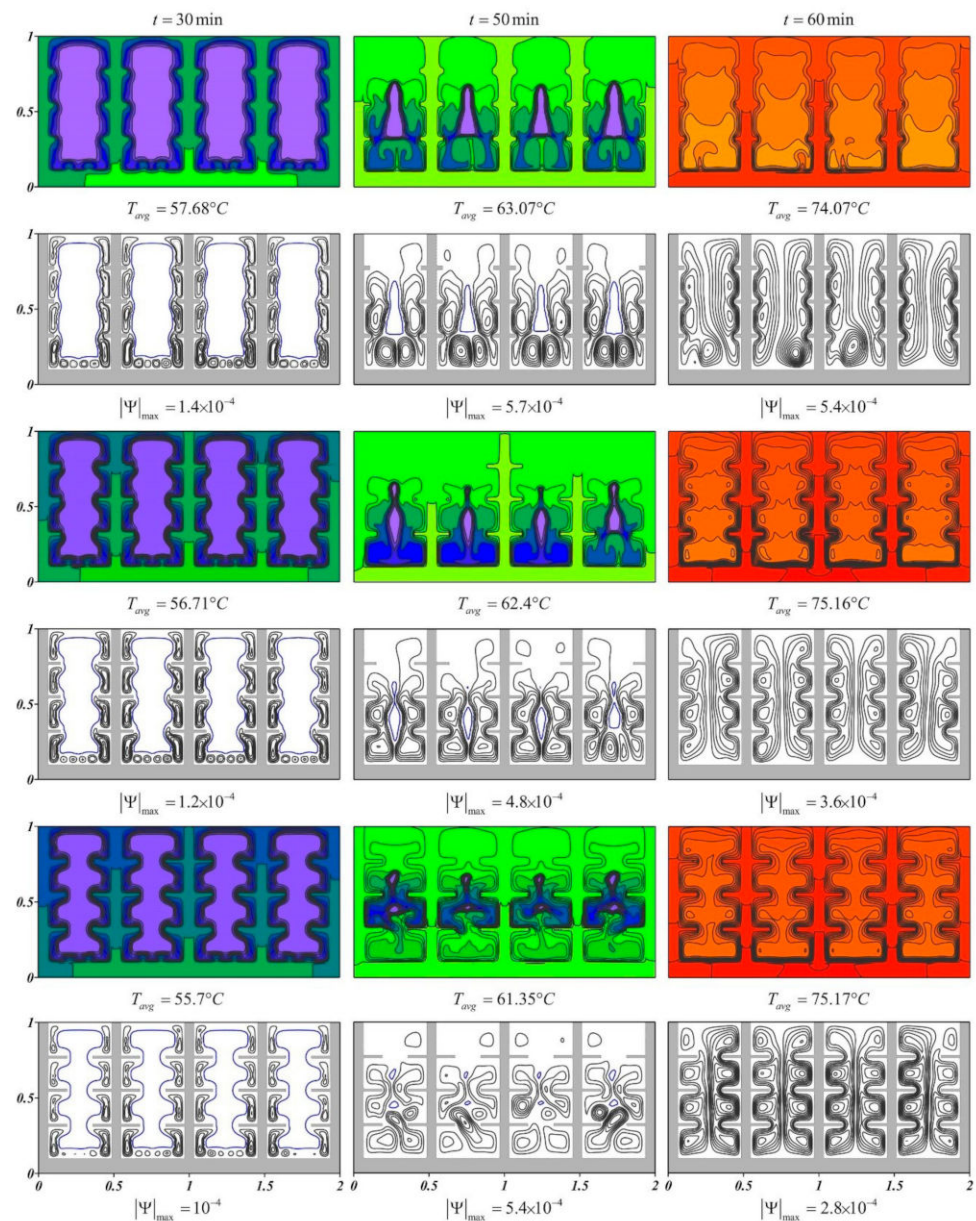


Figure 4. Temperature fields and isolines of the stream function at $Os = 0.169$ for the cases $l = H/24$, $l = H/12$, and $l = H/8$ at the time moments $t = 30$, $t = 50$, and $t = 60$ min.

The distribution of isotherms inside the copper profile shows that heat inside the metal spreads very quickly. A thickening of isotherms is observed on the surface of fins;

a high heat flux is associated with the beginning of the melting process. Heat dissipation occurs due to the phenomenon of thermal conductivity over the entire inner surface, and a uniform melt layer appears along with the entire height. Simultaneously, small convective recirculation occurs between the zone of unmelted material and the heating area. The acid melting in the lower part occurs mainly due to the ascending heat fluxes from the base of the cooler, the heated melt accumulates in the upper part. After 50 min of the source operation, a small portion of solid material remains in the central part of each reservoir.

In the course of melting, the area of action of convective heat transfer grows and deforms, and depending on the streamlines shape of the profile, the hydrodynamic picture changes. The large dimensions of the PCM cavities promote the formation of complex flow structures, and the slight change in the length of the transverse fins affects the energy transference between the cooler and lauric acid. A slight elongation of the fins causes the circulation cells to separate, which makes it difficult for the melt to move along the entire height of the cavities. Further, if at small l a more or less symmetrical picture is observed, then the elongation of the fins leads to destabilization of convective flows and unsteadiness of the vortex structure.

An increase in the length of the horizontal fins leads to a decrease in the volume fraction of phase change material, in heat sinks without transverse fins, the volume fraction of PCM is 75%, in the case of $l = H/24$, $l = H/12$, and $l = H/8$, the volume fraction of lauric acid decreases to 73.5%, 72%, and 70.5% of the total volume of cooling element, respectively. Along with a decrease in the mentioned proportion of PCM, the contact area of the material and the heat sink increases significantly: the contact surface increases by 25%, 50%, and 75% for $l = H/24$, $l = H/12$, and $l = H/8$ respectively, compared to heat sink with only vertical fins ($l = 0$).

The behavior of the average heater temperature (T_{avg}) reflects the efficiency of energy absorption by PCM (see Figure 5). The red profiles illustrate the results without natural convection influence. The intensification of convective phenomenon begins after an appearance of a small volume of melt, which is noticeably reflected in the average heater temperature after 22 min of heating. The temperature of the heater in the model without taking into account convective heat and mass transfer occurs monotonously, while the difference with natural convection process reaches 14 degrees in the absence of horizontal ribs. In the case of $l = H/8$, the difference in T_{avg} approaches 10 degrees at 50 min. The phenomenon of convective heat transfer in this case has a significant effect on the melting process and must be taken into account in simulation when the interface moves away from the highly heat-conducting surface of the profile.

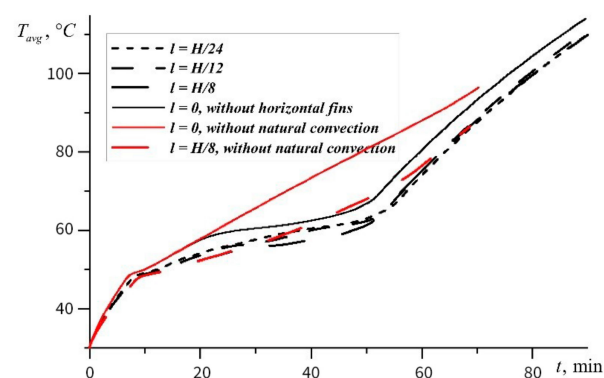


Figure 5. The rise in the average source temperature for the Ostrogradsky number $Os = 0.169$.

It should be noted that from the beginning of heating, a monotonic and uniform increase in temperature occurs. Over time, a small difference begins to be detected associated with the volume fraction of the copper profile, the density of which is much higher than the other system components. Conventional heat sink with only vertical fins shows the highest source temperatures during the melting process, as well as after the material has

completely melted. The temperature difference for cases $l = 0$ and $l = H/8$ practically reaches 5 degrees. After the heater temperature reaches the melting point of lauric acid $T = 46\text{ }^{\circ}\text{C}$, the increase in T_{avg} slows down. The process of transformation of sensible heat into latent heat begins, in which most of the energy is spent on phase transformation. With the emergence and development of the melt zone, the dependence of the source temperature on the geometric characteristics of the profile appears and increases with time. The greatest effect is seen with an elongation, namely, for $l = H/8$, the temperature in the heater after 40 min of heating is lower by 2.9 degrees compared to the case for $l = H/24$. However, increasing the surface area of the heat sink characterizes an intensification of melting process. After the zone of solid PCM disappears completely, T_{avg} again begins to increase rapidly and monotonously, while the temperature of the heater becomes the same for each case.

Increasing the heat load up to $Os = 0.338$ (see Figure 6) accelerates the heating process of the metal surface, rising the temperature drop, and at the very beginning of the melting process, the melt zone is divided into smaller vortex cells.

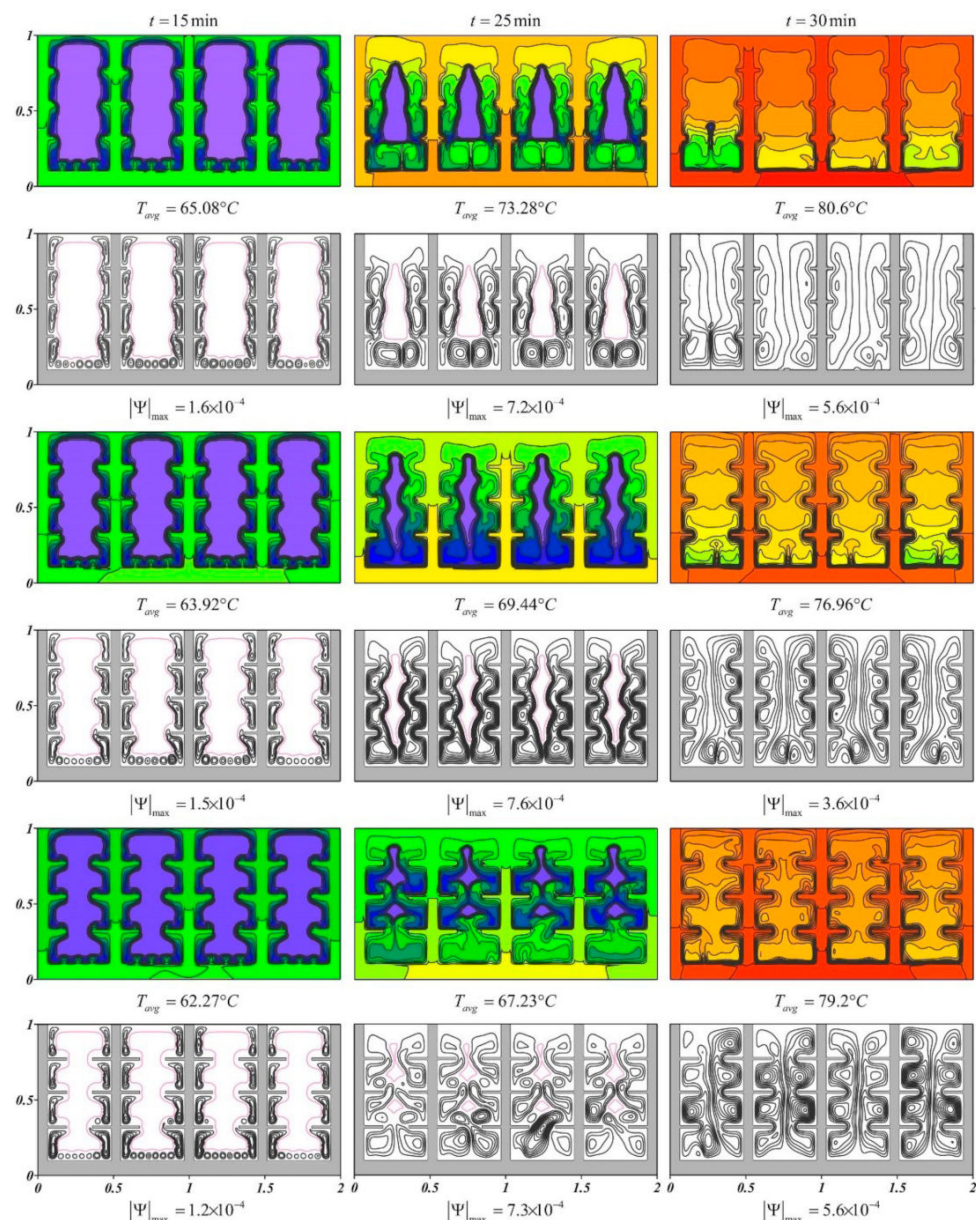


Figure 6. Temperature fields and streamlines at $Os = 0.338$ for the cases of $l = H/24$, $l = H/12$, and $l = H/8$ at the time moments $t = 15$, $t = 25$, and $t = 30$ min.

As in the case of $Os = 0.169$, the lengthening of the horizontal plate fins characterizes an essential contribution to the formation of convective flows. At $t = 25$ min, the largest volume of unmelted material is observed in the case of $l = H/24$. With such a length of small ribs, the main part of the melt circulates over the entire height of the region. It can be seen that the warmed melt is found in the upper part, which slows down phase transitions and promotes an increase in the plate temperature. At $t = 25$ min, the difference in the average temperatures of the source T_{avg} for the cases $l = H/24$ and $l = H/8$ exceeds 6 degrees. After PCM is completely melted, this difference diminished due to reduced melting time at large values of l (Table 2).

The greatest effect of interaction between thermogravitational flows and the geometric shape of the heat sink is observed at higher thermal powers of the source (see Figure 7).

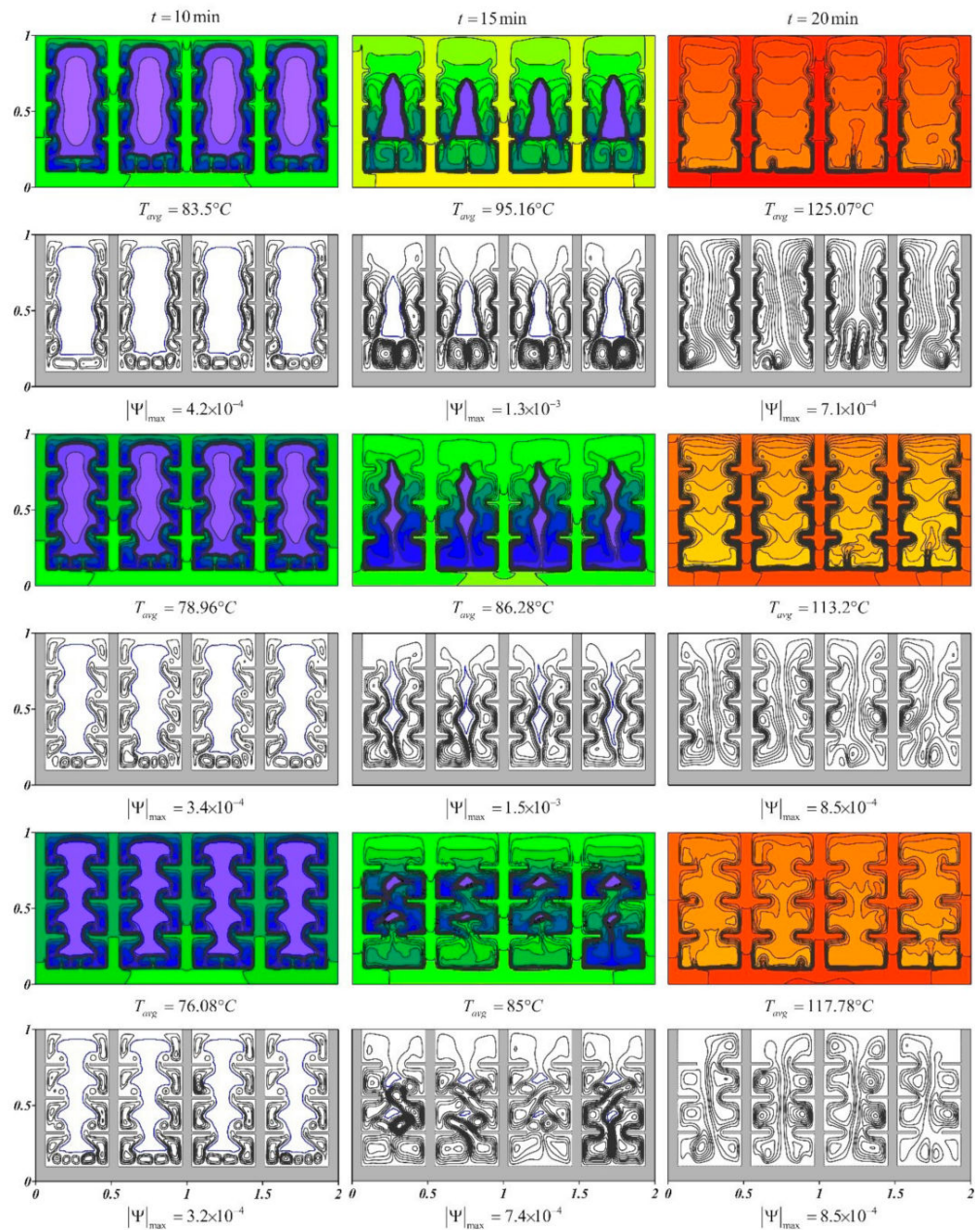


Figure 7. Temperature fields and streamlines at $Os = 0.676$ for the cases $l = H/24$, $l = H/12$, and $l = H/8$ at the time moments $t = 10$, $t = 15$, and $t = 20$ min.

As in the previous cases, a more uniform melting of the material along the height should be noted for heat sinks with elongated fins. Despite the decrease in the proportion of PCM, a growth of the size of the transverse plate fins results in a decrease in the average heater temperature owing to a raise of energy dissipation. At $t = 10$ min for $l = H/12$ and $l = H/8$, the average temperature in the source reaches 78.96 and 76.08 degrees, respectively, which is 4.54 and 7.42 lower than in the case of $l = H/24$. At time $t = 15$ min, this difference reaches 10 degrees, which reflects a significant contribution to the performance of PCM-based cooler.

It should be noted that in the case of $l = H/24$, closed cells are formed on the surface of the main plate, circulating only in the lower part, while the elongation of the transverse ribs to $l = H/12$ results to the formation of central descending circulations of the cold melt. In this way, the temperature of the slab is significantly reduced.

Table 2. Melting time for different Ostrogradsky numbers.

| Ostrogradsky Number | Length of Horizontal Fins | | |
|---------------------|---------------------------|-------------|-------------|
| | $l = H/24$ | $l = H/12$ | $l = H/8$ |
| 0.169 | 55 min | 53 min 9 s | 51 min 30 s |
| 0.338 | 30 min 9 s | 29 min 20 s | 27 min 45 s |
| 0.676 | 17 min 23 s | 17 min 7 s | 16 min 4 s |

Figure 8 demonstrates the dynamic change in the mean heater temperature at $Os = 0.676$. The high intensity of heat generation characterizes the rapid heating of the radiator system. However, the contact area has an essential impact on the energy exchange of the metal with a less heat-conducting material. Already 2 min after switching on the element, the effect of adding transverse fins appears. With such an intensity of heat generation, the temperature difference between a case of standard heat sink without transverse fins and the case of $l = H/8$ exceeds 12 degrees at time $t = 10$ min. If in the first minutes the influence is associated with the phenomenon of thermal conductivity and is proportional to the change in the surface area, then with a rise in the melt zone and the development of convective energy and mass transference in it, the temperature in the source at $l = H/12$ and $l = H/8$ becomes the same, while T_{avg} in the case of $l = H/24$ begins to increase. This phenomenon is primarily associated with a change in the hydrodynamics of the melt affected the addition of transverse fins.

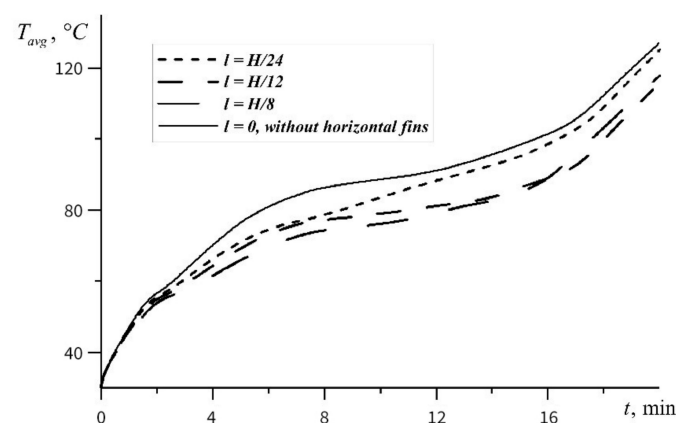


Figure 8. The graph of the dependence of the mean heater temperature on time at $Os = 0.676$.

5. Conclusions

In passive cooling systems based on phase change materials at high thermal loads, convective energy and mass transference plays an essential role. In this study, the influence of the geometric shape of the heat sink filled with lauric acid on the heat dissipation and melting was evaluated. It has been shown that a growth of the length of the transverse fins

contributes to a decrease in the temperature of the source owing to a raise of the surface area at the initial stages of heating, as well as due to hydrodynamic features as the molten material volume increases. The elongation of the baffles promotes a more uniform melting of the material over the entire height of the region, as well as the formation of descending flows of cooled melt that cool the bottom heat sink plate. It was shown that at high thermal loads ($Os = 0.676$), heat sink design changed by adding horizontal fins allows increasing the surface area by 75% and reducing the heater temperature by 12 degrees, while for a heat load of $Os = 0.169$, a decrease in the average heater temperature by 5 degrees is observed.

The absence of transverse fins or their short length leads to the accumulation of heated melt in the upper part of the sink, which results in a diminution of energy transference with the metal profile. The rise of the size of the additional fins intensifies the mixing of the liquid so that the melting occurs more evenly along with the height of the region. At high heat loads, the temperature in the heating element can be reduced by more than 10 degrees by increasing the length of the transverse fins.

During the melting of the material, the average heater temperature does not exceed 80 °C for $l \geq H/12$ at $Os = 0.676$ and 60 °C at $Os = 0.169$. After the material was completely melted, the additional fins also provide more intense heat exchange with the material, significantly reducing the heater temperature.

Author Contributions: N.S.B. and M.A.S. conceived the main concept. N.S.B. and M.A.S. contributed to the investigation and data analysis. N.S.B., M.G., and M.A.S. wrote the manuscript. All authors contributed in writing the final manuscript. All authors have read and agreed to the published version of the manuscript.

Funding: This work was supported by the Grants Council (under the President of the Russian Federation), Grant No. MK-1934.2019.1.

Institutional Review Board Statement: Not applicable.

Informed Consent Statement: Not applicable.

Data Availability Statement: Data is contained within this article.

Conflicts of Interest: The authors declare no conflict of interest.

Abbreviations

The following abbreviations are used in this manuscript:

| | |
|--------|---|
| Bi | Biot number |
| c | specific heat, $\text{JK}^{-1} \text{kg}^{-1}$ |
| g | gravity acceleration, ms^{-2} |
| H | chamber size, m |
| h | specific enthalpy, Jkg^{-1} |
| k | heat conductivity, $\text{WK}^{-1}\text{m}^{-1}$ |
| L | cavity length, m |
| L_f | fusion energy or latent heat of melting, Jkg^{-1} |
| Os | Ostrogradsky number |
| p | pressure, Pa |
| Pr | Prandtl number |
| Q | energy production strength per unit of volume, W m^{-3} |
| Ra | Rayleigh number |
| Ste | Stefan number |
| t | time, s |
| T | temperature, K |
| T_m | melting temperature, K |
| u, v | velocity projections in Cartesian coordinate along x and y , ms^{-1} |
| U, V | non-dimensional velocity projections |
| x, y | Cartesian coordinates, m |
| X, Y | non-dimensional Cartesian coordinates |

Greek symbols

| | |
|-----------|--|
| α | heat diffusivity, $\text{m}^2 \text{s}^{-1}$ |
| β | coefficient of thermal expansion, K^{-1} |
| γ | energy transference coefficient, $\text{WK}^{-1}\text{m}^{-2}$ |
| η | smoothing characteristic (or melting temperature range), K |
| Θ | non-dimensional temperature |
| μ | dynamic viscosity, Pa s |
| ν | kinematic viscosity, $\text{m}^2 \text{s}^{-1}$ |
| ρ | density, kgm^{-3} |
| τ | non-dimensional time |
| φ | volume fraction of the melt |
| ψ | stream function, $\text{m}^2 \text{s}^{-1}$ |
| Ψ | non-dimensional stream function |
| ω | vorticity, s^{-1} |
| Ω | non-dimensional vorticity |

Subscripts

| | |
|-----|------------------------------|
| 0 | initial condition or ambient |
| 1 | cooler |
| 2 | heated unit |
| l | liquid |
| m | melting |
| s | solid |

References

- Alam, M.W.; Bhattacharyya, S.; Souayah, B.; Dey, K.; Hammami, F.; Rahimi-Gorji, M.; Biswas, R. CPU heat sink cooling by triangular shape micro-pin-fin: Numerical study. *Int. Commun. Heat Mass Transf.* **2020**, *112*, 104455. [[CrossRef](#)]
- Hosseinirad, E.; Khoshvaght-Aliabadi, M.; Hormozi, F. Effects of splitter shape on thermal-hydraulic characteristics of plate-pin-fin heat sink (PPFHS). *Int. J. Heat Mass Transf.* **2019**, *143*, 118586. [[CrossRef](#)]
- Mandal, P.K.; Sengupta, S.; Rana, S.C.; Bhanja, D. Effect of orientation angle in thermal performance analysis of a horizontal heat sink of perforated pin fins. *Aip Conf. Proc.* **2019**, *2148*, 030003.
- Kim, S.J.; Kim, D.-K.; Oh, H.H. Comparison of fluid flow and thermal characteristics of plate-fin and pin-fin heat sinks subject to a parallel flow. *Heat Transf. Eng.* **2008**, *29*, 169–177. [[CrossRef](#)]
- Iasiello, M.; Bianco, N.; Chiu, W.K.S.; Naso, V. The effects of variable porosity and cell size on the thermal performance of functionally-graded foams. *Int. J. Therm. Sci.* **2021**, *160*, 106696. [[CrossRef](#)]
- Andreozzi, A.; Bianco, N.; Iasiello, M.; Naso, V. Numerical study of metal foam heat sinks under uniform impinging flow. *IOP Conf. Ser. J. Phys.* **2017**, *796*, 012002. [[CrossRef](#)]
- Bianco, N.; Iasiello, M.; Mauro, G.M.; Pagano, L. Multi-objective optimization of finned metal foam heat-sinks: Tradeoff between heat transfer and pressure drop. *Appl. Therm. Eng.* **2021**, *182*, 116058. [[CrossRef](#)]
- Feng, S.S.; Kuang, J.J.; Lu, T.J.; Ichimiya, K. Heat transfer and pressure drop characteristics of finned metal foam heat sinks under uniform impinging flow. *J. Electron. Packag.* **2015**, *137*, 021014. [[CrossRef](#)]
- Setoh, G.; Tan, F.L.; Fok, S.C. Experimental studies on the use of a phase change material for cooling mobile phones. *Int. Commun. Heat Mass Transf.* **2010**, *37*, 1403–1410. [[CrossRef](#)]
- Sharifi, N.; Bergman, T.L.; Faghri, A. Enhancement of PCM melting in enclosures with horizontally-finned internal surfaces. *Int. J. Heat Mass Transf.* **2011**, *54*, 4182–4192. [[CrossRef](#)]
- Xie, J.; Choo, K.F.; Xiang, J.; Lee, H.M. Characterization of natural convection in a PCM-based heat sink with novel conductive structures. *Int. Commun. Heat Mass Transf.* **2019**, *108*, 104306. [[CrossRef](#)]
- Lv, Y.; Yang, X.; Li, X.; Zhang, G.; Wang, Z.; Yang, C. Experimental study on a novel battery thermal management technology based on low density polyethylene-enhanced composite phase change materials coupled with low fins. *Appl. Energy* **2016**, *178*, 376–382. [[CrossRef](#)]
- Kenisarin, M.; Mahkamov, K. Solar energy storage using phase change materials. *Renew. Sustain. Energy Rev.* **2007**, *11*, 1913–1965. [[CrossRef](#)]
- Abhat, A. Low temperature latent heat thermal energy storage: Heat storage materials. *Sol. Energy* **1983**, *10*, 313–332. [[CrossRef](#)]
- Yousef, M.S.; Hassan, H.; Kodama, S.; Sekiguchi, H. An experimental study on the performance of single slope solar still integrated with a PCM-based pin-finned heat sink. *Energy Procedia* **2019**, *56*, 100–104. [[CrossRef](#)]
- Zhou, Z.; Zhang, Z.; Zuo, J.; Huang, K.; Zhang, L. Phase change materials for solar thermal energy storage in residential buildings in cold climate. *Renew. Sustain. Energy Rev.* **2015**, *48*, 692–703. [[CrossRef](#)]
- Iasiello, M.; Mameli, M.; Filippeschi, S.; Bianco, N. Simulations of paraffine melting inside metal foams at different gravity levels with preliminary experimental validation. *J. Phys. Conf. Ser.* **2020**, *1599*, 012008. [[CrossRef](#)]

18. Hasan, A.; McCormack, S.J.; Huang, M.J.; Sarwar, J.; Norton, B. Increased photovoltaic performance through temperature regulation by phase change materials: Materials comparison in different climates. *Sol. Energy* **2015**, *115*, 264–276. [[CrossRef](#)]
19. Sahoo, S.K.; Das, M.K.; Rath, P. Application of TCE-PCM based heat sinks for cooling of electronic components: A review. *Renew. Sustain. Energy Rev.* **2016**, *59*, 550–582. [[CrossRef](#)]
20. Avci, M.; Yazici, M.Y. An experimental study on effect of inclination angle on the performance of a PCM-based flat-type heat sink. *Appl. Therm. Eng.* **2018**, *131*, 806–814. [[CrossRef](#)]
21. Kalbasi, R.; Afrand, M.; Alsarraf, J.; Tran, M.-D. Studies on optimum fins number in PCM-based heat sinks. *Energy* **2019**, *171*, 1088–1099. [[CrossRef](#)]
22. Ali, H.M.; Ashraf, M.J.; Giovannelli, A.; Irfan, M.; Irshad, T.B.; Hamid, H.M.; Hassan, F.; Arshad, A. Thermal management of electronics: An experimental analysis of triangular, rectangular and circular pin-fin heat sinks for various PCMs. *Int. J. Heat Mass Transf.* **2018**, *123*, 272–284. [[CrossRef](#)]
23. Fan, L.-W.; Xiao, Y.-Q.; Zeng, Y.; Fang, X.; Wang, X.; Xu, X.; Yu, Z.-T.; Hong, R.-H.; Hu, Y.-C.; Cen, K.-F. Effects of melting temperature and the presence of internal fins on the performance of a phase change material (PCM)-based heat sink. *Int. J. Therm. Sci.* **2013**, *70*, 114–126. [[CrossRef](#)]
24. Ghanbarpour, A.; Hosseini, M.J.; Ranjbar, A.A.; Rahimi, M.; Bahrampoury, R.; Ghanbarpour, M. Evaluation of heat sink performance using PCM and vapor chamber/heat pipe. *Renew. Energy* **2021**, *163*, 698–719. [[CrossRef](#)]
25. Pakrouh, R.; Hosseini, M.J.; Ranjbar, A.A.; Bahrampoury, R. A numerical method for PCM-based pin fin heat sinks optimization. *Energy Convers. Manag.* **2015**, *103*, 542–552. [[CrossRef](#)]
26. Ali, H.M.; Arshad, A.; Janjua, M.M.; Baig, W.; Sajjad, U. Thermal performance of LHSU for electronics under steady and transient operations modes. *Int. J. Heat Mass Transf.* **2018**, *127*, 1223–1232. [[CrossRef](#)]
27. Pakrouh, R.; Hosseini, M.J.; Ranjbar, A.A. A parametric investigation of a PCM-based pin fin heat sink. *Mech. Sci.* **2015**, *6*, 65–73. [[CrossRef](#)]
28. Arshad, A.; Ali, H.M.; Ali, M.; Manzur, S. Thermal performance of phase change material (PCM) based pin-finned heat sinks for electronics devices: Effect of pin thickness and PCM volume fraction. *Appl. Therm. Eng.* **2017**, *112*, 143–155. [[CrossRef](#)]
29. Dammak, K.; El Hami, A. Thermal reliability-based design optimization using Kriging model of PCM based pin fin heat sink. *Int. J. Heat Mass Transf.* **2021**, *166*, 120745. [[CrossRef](#)]
30. Srikanth, R.; Balaji, C. Experimental investigation on the heat transfer performance of a PCM based pin fin heat sink with discrete heating. *Int. J. Therm. Sci.* **2017**, *111*, 188–203. [[CrossRef](#)]
31. Saha, S.K.; Dutta, P. Heat transfer correlations for PCM-based heat sinks with plate fins. *Appl. Therm. Eng.* **2010**, *30*, 2485–2491. [[CrossRef](#)]
32. Wang, G.; Wei, G.; Xu, C.; Ju, X.; Yang, Y.; Du, X. Numerical simulation of effective thermal conductivity and pore-scale melting process of PCMs in foam metals. *Appl. Therm. Eng.* **2019**, *147*, 464–472. [[CrossRef](#)]
33. El Idi, M.M.; Karkri, M. Heating and cooling conditions effects on the kinetic of phase change of PCM embedded in metal foam. *Case Stud. Therm. Eng.* **2020**, *21*, 100716. [[CrossRef](#)]
34. Dinesh, B.V.S.; Bhattacharya, A. Comparison of energy absorption characteristics of PCM-metal foam systems with different pore size distributions. *J. Energy Storage* **2020**, *28*, 101190. [[CrossRef](#)]
35. Rehman, T.; Ali, H.M.; Saieed, A.; Pao, W.; Ali, M. Copper foam/PCMs based heat sinks: An experimental study for electronic cooling systems. *Int. J. Heat Mass Transf.* **2018**, *127*, 381–393. [[CrossRef](#)]
36. Sardari, P.T.; Babaie-Mahani, R.; Giddings, D.; Yasserli, S.; Moghimi, M.A.; Bahai, H. Energy recovery from domestic radiators using a compact composite metal Foam/PCM latent heat storage. *J. Clean. Prod.* **2020**, *257*, 120504. [[CrossRef](#)]
37. Buonomo, B.; Ercole, D.; Manca, O.; Nardini, S. Thermal behaviors of latent thermal energy storage system with PCM and aluminum foam. *Int. J. Heat Technol.* **2016**, *34*, 359–364. [[CrossRef](#)]
38. Qu, Z.G.; Li, W.Q.; Wang, J.L.; Tao, W.Q. Passive thermal management using metal foam saturated with phase change material in a heat sink. *Int. Commun. Heat Mass Transf.* **2012**, *39*, 1546–1549. [[CrossRef](#)]
39. Zhu, F.; Zhang, C.; Gong, X. Numerical analysis on the energy storage efficiency of phase change material embedded in finned metal foam with graded porosity. *Appl. Therm. Eng.* **2017**, *123*, 256–265. [[CrossRef](#)]
40. Hu, C.; Li, H.; Tang, D.; Zhu, J.; Wang, K.; Hu, X.; Bai, M. Pore-scale investigation on the heat-storage characteristics of phase change material in graded copper foam. *Appl. Therm. Eng.* **2020**, *178*, 115609. [[CrossRef](#)]
41. Baby, R.; Balaji, C. Thermal optimization of PCM based pin fin heat sinks: An experimental study. *Appl. Therm. Eng.* **2013**, *54*, 65–77. [[CrossRef](#)]
42. Bondareva, N.S.; Sheremet, M.A. Conjugate heat transfer in the PCM-based heat storage system with finned copper profile: Application in electronics cooling. *Int. J. Heat Mass Transf.* **2018**, *124*, 1275–1284. [[CrossRef](#)]
43. Bondareva, N.S.; Sheremet, M.A. Effect of inclined magnetic field on natural convection melting in a square cavity with a local heat source. *J. Magn. Magn. Mater.* **2016**, *419*, 476–484. [[CrossRef](#)]
44. Kamkari, B.; Groulx, D. Experimental investigation of melting behavior of phase change material in finned rectangular enclosures under different inclination angles. *Exp. Therm. Fluid Sci.* **2018**, *97*, 94–108. [[CrossRef](#)]
45. Bondareva, N.S.; Gibanov, N.S.; Sheremet, M.A. Computational study of heat transfer inside different PCMs enhanced by Al₂O₃ nanoparticles in a copper heat sink at high heat loads. *Nanomaterials* **2020**, *10*, 284. [[CrossRef](#)] [[PubMed](#)]
46. Gau, C.; Viskanta, R. Melting and solidification of a pure metal on a vertical wall. *J. Heat Transf.* **1986**, *108*, 174–181. [[CrossRef](#)]